

Evidence for a resonant cyclotron line in IGR J16493–4348 from the Swift-BAT hard X-ray survey

A.D’Ai¹, G. Cusumano², V. La Parola², A. Segreto², T. Di Salvo¹, R. Iaria¹, N.R. Robba¹

¹ Dipartimento di Fisica, Università di Palermo, Via Archirafi 36, I-90123, Palermo, Italy e-mail: antonino.dai@unipa.it

² INAF, Istituto di Astrofisica Spaziale e Fisica Cosmica, Via U. La Malfa 153, I-90146 Palermo, Italy

Abstract

Context. Resonant absorption cyclotron features are a key diagnostic tool to directly measure the strength of the magnetic field of accreting neutron stars. However, typical values for cyclotron features lie in the high-energy part of the spectrum between 20 keV and 50 keV, where detection is often damped by the low statistics from single pointed observations.

Aims. We show that long-term monitoring campaign performed with Swift-BAT of persistently, but faint, accreting high-mass X-ray binaries is able to reveal in their spectra the presence of cyclotron features.

Methods. We extracted the average Swift-BAT 15–150 keV spectrum from the 54 months long Swift-BAT survey of the high-mass X-ray source IGR J16493–4348. To constrain the broadband spectrum we used soft X-ray spectra from Swift-XRT and Suzaku pointed observations.

Results. We model the spectra using a set of phenomenological models usually adopted to describe the energy spectrum of accreting high-mass X-ray binaries; irrespective of the models we used, we found significant improvements in the spectral fits adding to the models a broad (10 keV width) absorption feature, with best-fitting energy estimate between 30 and 33 keV, that we interpret as evidence for a resonant cyclotron absorption feature. We also discuss instrumental issues related to the use of Swift-BAT for this kind of studies and the statistical method to weight the confidence level of this detection. Correcting for the gravitational redshift of a 1.4 M_{\odot} neutron star, the inferred surface magnetic field is $B_{\text{surf}} \sim 3.7 \times 10^{12}$ Gauss. The spectral parameters of IGR J16493–4348 fit well with empirical correlations observed when the whole sample of high-mass binaries with detected cyclotron features is considered.

Key words. X-rays: binaries – X-rays: individual: IGR J16493–4348.

1. Introduction

The Burst Alert Telescope (BAT, Barthelmy et al. 2005) on board Swift (Gehrels et al. 2004) has been performing a continuous monitoring of the sky in the hard X-ray energy range (15–150 keV) since November 2004. The telescope, thanks to its large field of view (1.4 steradian half coded) and its pointing strategy, covers a fraction between 50% and 80% of the sky every day. This has allowed the detection of many of the new INTEGRAL High-Mass X-ray Binaries (HMXBs, e.g. Cusumano et al. 2010b) and the collection of their long term light curves and spectra. The long and continuous monitoring of these sources allows to investigate the intrinsic emission variability, to search for long periodicities (orbital periods) and to discover the presence of eclipse events. The role of Swift-BAT (hereafter simply BAT) is therefore fundamental to unveil the nature and the geometry of these binary systems. Moreover BAT collects their long-term averaged energy spectra in the 15.0–150 keV band. For HMXBs this energy range is extremely important as resonant cyclotron scattering features (CRSFs) are usually observed in this part of the X-ray spectrum (Heindl et al. 2004).

In this paper we analyse the soft and hard X-ray data collected by BAT, INTEGRAL and by pointed Suzaku and Swift-XRT observations on IGR J16493–4348. This source was discovered by INTEGRAL in 2004 (Bird et al. 2004) and it was initially associated with the radio pulsar PSR J1649–4349 because of a spatial coincidence. A later INTEGRAL observation with a deep exposure allowed to reduce the positional uncertainty and to reject the pulsar association (Grebenev et al. 2005). A follow-up observation with *Chandra* found a soft X-ray coun-

terpart at a position of RA(J2000) = 16°49′26.92″; Dec(J2000) = -43°49′8.96″ (Kuiper et al. 2005) allowing the association with the infrared counterpart 2MASS J1642695–4349090, a B0.5 Ib supergiant. Nespoli et al. (2010) performed K-band spectroscopy of the inferred counterpart, confirming the B0.51 Ia-Ib companion spectral type; the infrared extinction, translated into the equivalent hydrogen column density, was estimated to be $(2.92 \pm 1.96) \times 10^{22} \text{ cm}^{-2}$, a value that is lower with respect to the X-ray absorption, thus indicating that part of the X-ray absorption may be local to the compact object. Cusumano et al. (2010a) found a periodicity of 6.732 ± 0.002 d, interpreted as the orbital period of the system. The folded light curve shows presence of an eclipse, lasting $\sim 12\%$ of the P_{orb} . Assuming a 1.4 M_{\odot} neutron star (NS) and 32 R_{\odot} for the companion star, the system has most likely a low eccentricity value ($e \leq 0.15$). Recently, Corbet et al. (2010) found in RXTE observations evidence for a shorter periodicity at 1069 ± 7 s, interpreted as the NS spin period.

A spectral analysis using non simultaneous data from Swift-XRT and INTEGRAL (Hill et al. 2008) showed that the broadband X-ray spectrum could be well fitted by an absorbed ($N_{\text{H}} = 5.6 \times 10^{22} \text{ cm}^{-2}$) power-law ($\Gamma = 0.6 \pm 0.3$) with a high-energy cut-off at ~ 17 keV. Morris et al. (2009) analysing Suzaku data of IGR J16493–4348, proposed an alternative modelling of the X-ray spectrum using a partial covering component multiplied by a simple power-law. The covering fraction of the total emission was estimated in 0.62 ± 0.07 , while the local value of the N_{H} was estimated in $\sim 30 \times 10^{22} \text{ cm}^{-2}$.

2. Data Reduction

The raw BAT survey data of the first 54 months of the Swift mission were retrieved from the HEASARC public archive¹ and processed with a dedicated software (Segreto et al. 2010), that performs screening, mosaicking and source detection on BAT data and produces spectra and light curves for any given sky position. The light curve of IGR J16493–4348 was extracted in the 15–150 keV energy range with the maximum available time resolution (~ 300 s). The spectrum was obtained by extracting the source count rates in 16 energy bands and analysed using the BAT spectral redistribution matrix². The last three energy channels (100–150 keV range) were rebinned into a single channel in order to have a S/N ratio above 3σ . The source is detected at a significance level of ~ 21 standard deviations. The average count rate in the BAT light curve is 1.03×10^{-4} count s^{-1} pixel $^{-1}$. When considering the light curve at the highest resolution the maximum of the deviation from the average rate is about 7σ , corresponding to an increase in rate of a factor ~ 20 . Although the count rate indicates brightness variations in the accreting source, we found no evidence for spectral shape variability, when spectra collected on one month time span were fitted using a simple power-law model, with photon indices consistent with the average value within the errors. The 15–50 keV and 50–150 keV time-averaged fluxes are $(3.0 \pm 0.3) \times 10^{-11}$ erg cm^{-2} s^{-1} and $(1.4^{+0.1}_{-0.3}) \times 10^{-11}$ erg cm^{-2} s^{-1} , respectively.

We analysed also INTEGRAL-ISGRI (hereafter simply ISGRI) long-term data obtained from the Integral high-level products archive HEAVENS³. ISGRI data were used in the 15–150 keV energy range.

To have the necessary coverage of the soft X-ray band we used data of the Swift-XRT (hereafter simply XRT, Burrows et al. 2005) observation performed on 2006 March 11 (Obs.ID 00030379002), for a total exposure time of 5.6 ks and a Suzaku (Mitsuda et al. 2007) observation performed on 2006 October 10 (Obs.ID 401054010, see Morris et al. 2009, for further details).

The XRT data were processed with standard procedures (XRTPIPELINE v.0.12.4), filtering and screening criteria, using FTOOLS in the HEASOFT package (v 6.8). The source was observed in Photon Counting mode (Hill et al. 2004). We adopted standard grade filtering 0–12. The source events for spectral analysis were extracted from a circular region of 20 pixels radius (1 pixel=2.36”) centred on the source position as determined with XRTCENTROID. The background was extracted from an annular region centred on the source with radii of 70 and 130 pixels, respectively. The spectrum was analysed using ancillary response files generated with XRTMKARF and spectral redistribution matrix v011.

We extracted Suzaku scientific data (Obs.ID 401054010) from clean events reprocessed with the 2.0.6.13 standard pipeline procedure. We obtained four spectra from the X-ray Imaging Spectrometer (XIS(0–4), Koyama et al. 2007). Spectra from the front-illuminated CCD (XIS0, XIS2 and XIS3) were combined into a single spectrum (XIS023) using the *addas-caspec* script, while the XIS1 spectrum was used in the analysis as a different dataset.

The source extraction region was centred on the CHANDRA source position with a radius of 140”. Background region was obtained from an equal spatial region adjacent to the source

¹ <http://heasarc.gsfc.nasa.gov/docs/archive.html>

² <http://heasarc.gsfc.nasa.gov/docs/heasarc/caldb/data/swift/bat/index.html>

³ <http://www.isdc.unige.ch/heavens/>

region. Data from the HXD/PIN instrument (Takahashi et al. 2007) were obtained using the *hxdpinxbpi* script. The HXD/PIN background is the sum of a time-variable instrumental background (non-X-ray background, NXB) induced by cosmic rays and trapped charged particles in the satellite orbit and the intrinsic cosmic background (cosmic X-ray background, CXB). We used the 2.0 version of the *tuned* NXB model spectrum released by the HXD instrument team (LCFITDT model, Fukazawa et al. 2009) and the CXB spectrum obtained from the Boldt (1987) X-ray background model convolved with the PIN response for the flat emission distribution at the epoch of this observation. Given the lack of local narrow features, spectra from XIS and HXD/PIN were coarsely rebinned into a spectrum of 84 (21) energy channels for the XIS023 (XIS1) and 9 energy channels for the HXD/PIN. This choice leaves a S/N ratio above 3 for each energy channel. XIS data are background dominated below 2 keV and above 10 keV, so that these channels were not used in the spectral analysis. HXD/PIN spectrum was used in the 12.0–40.0 keV energy range.

Spectral fits were performed using XSPEC v.12.6.0. Errors are at 90 % confidence level, if not stated otherwise.

3. Spectral Analysis

BAT data were collected during the monitoring campaign from 2004 December to 2009 May, ISGRI data from 2003 January to 2009 April, and they both track, within the same temporal window, the long-term average hard X-ray emission. Swift-XRT and Suzaku observations, as indicated in the previous section, are pointed observations taken at different times. In order to constrain the broadband spectrum we distinguished, therefore, the two soft X-ray observations performed with XRT and Suzaku. For *Spectrum 1*, we hereafter assume the spectrum containing the following datasets: XRT, BAT, ISGRI. For *Spectrum 2*, the spectrum composed of these datasets: Suzaku (XIS1, XIS023 and HXD/PIN), BAT and ISGRI.

We adopted an inter-calibration multiplicative constant to take into account flux uncertainties in the response of the different instruments. A common fit of the ISGRI and BAT data does not reveal any systematic flux mismatch. Data could satisfactorily be fitted using a power-law model and the residuals did not show any systematic difference in the two datasets. A calibration constant between the datasets (fixed to one for the BAT data and left free for the ISGRI data) was found to be consistent with one. Therefore, for the following analysis we fixed the inter-calibration factor between these two instruments to one.

For *Spectrum 1*, the constant was fixed to 1 for the XRT dataset and left free for the BAT/ISGRI datasets (C_{bat}). For *Spectrum 2*, the constant was fixed to 1 for the XIS023 spectrum and left free for the HXD-PIN dataset (C_{hxd}), for the XIS1 dataset (C_{xis1}) and for the BAT/ISGRI dataset (C_{bat}). The 1–10 keV absorbed/unabsorbed flux was $(5.26 \pm 0.08 / 8.15 \pm 0.15) \times 10^{-11}$ erg cm^{-2} s^{-1} for the Swift-XRT observation, whereas it was $(1.36 \pm 0.01 / 2.35 \pm 0.05) \times 10^{-11}$ erg cm^{-2} s^{-1} during the Suzaku observation (errorbars take also into account the uncertainty associated with different modelizations of the spectra).

To model the data, we employed the three most commonly used models to fit broadband spectra of accreting high-mass X-ray binaries (see Makishima et al. 1999, for a comprehensive discussion of the models): a cut-off power law model (model *cutoffpl*), a power-law with a Fermi-Dirac cut-off (model *fdco*), the negative-positive power-law model (model *npex*, with the positive photon index fixed to +2). The *cutoffpl*

model has three main parameters: the photon-index (Γ), the cut-off energy (E_{cut}), the normalization of the power-law (N_{po}); the `fdco` model has one more parameter, the folding energy of the power-law (E_{fol}); the `npex` is basically the sum of two power-laws with a common exponential cut-off.

We did not use the partial covering model of a power-law spectrum as in Morris et al. (2009), because this model is not physically consistent with the nature of IGR J16493–4348, as the 6.732 d orbital period and the 1069 s spin period place unambiguously IGR J16493–4348 in the wind-fed HMXB zone of the $P_{\text{orb}}-P_{\text{spin}}$ diagram (also known as the Corbet diagram, Corbet 1984).

3.1. Spectrum 1

In the first column of Table 1, we present the best-fitting results adopting our set of spectral models for the *Spectrum 1* datasets.

The absorbed power-law with a high energy exponential cut-off gives a column density $N_{\text{H}} = (7.0 \pm 1.2) \times 10^{22} \text{ cm}^{-2}$, $\Gamma = 0.7 \pm 0.3$ and a cut-off energy $E_{\text{cut}} = 20 \pm 5 \text{ keV}$. This model already proposed in Hill et al. (2008) is a better representation of the data with respect to the more sophisticated `fdco` model, but we found that the `npex` model provides still a better fit to the data, even if the steepness of the power-law, the cut-off energy and the N_{H} are consistent in the two models. Irrespective of the model adopted, broad residuals were evident between 30 and 40 keV (see Fig. 1). Inspecting the data, we noted that the residuals were mostly driven by the residuals of the BAT data, because of the better S/N ratio of these data in the hard X-ray band. We have tentatively identified the shape of the residuals with a broad feature in absorption and we repeated the fits introducing a cyclotron absorption feature (`cyclabs` component, second column in Table 1), which is expressed according to the formula:

$$\text{CYCLABS}(E) = D_c \frac{(W_c E / E_c)^2}{(E - E_c)^2 + W_c^2} \quad (1)$$

where E_c , D_c and W_c are the cyclotron energy, depth and width respectively (Makishima et al. 1990). We assume that the broad feature constitute the fundamental and, given the low S/N at higher energies, we neglect higher harmonics.

The line parameters could not be all adequately constrained. We found that the width of the line strongly correlated with the cut-off energy of the continuum models, resulting in a large uncertainty. We, therefore, kept this parameter frozen to the value of 10 keV, as this was the most reasonable value that provided the lowest χ^2 in all the models adopted. This choice will also be discussed *a posteriori*. The energy of the line, for the `npex` best-fitting model is $33 \pm 4 \text{ keV}$, while the depth of the line is 0.5 ± 0.2 . Similar values were found also adopting the other two models, indicating a weak correlation with the broadband shape of the continuum. The addition of this component significantly improved the fit (reduced χ^2 1.16 against a value of 1.32 without the line). To fit CRSFs, a Gaussian absorption model (`gabs` in Xspec) has been often also used (Coburn et al. 2002). Replacing the `cyclabs` with the `gabs` model, did not significantly change the conclusions of our analysis. We found again a tight correlation between depth and σ of the line. The best-fitting position of the line varied, according to the model adopted, between 31 keV and 35 keV. Keeping the line σ frozen at 5 keV, the best-fitting depth of the line was found between 1 and 5. Relative errors on the best-fitting parameters were of the same order of the corresponding `cyclabs` analogues. The χ^2 values

Table 1. Spectral fitting results

	Spectrum1		Spectrum2	
	No cyc	+Cyc	No cyc	+Cyc
	cut off fpl			
N_{H}	$7.0^{+1.5}_{-1.2}$	$5.5^{+1.5}_{-0.8}$	$7.7^{+0.4}_{-0.5}$	7.5 ± 0.4
Γ	0.7 ± 0.3	$0.4^{+0.4}_{-0.2}$	1.1 ± 0.1	1.13 ± 0.12
$N_{\text{po}} (10^{-3})$	$5.4^{+4}_{-2.0}$	$2.7^{+2.5}_{-0.8}$	2.5 ± 0.5	2.4 ± 0.4
$E_{\text{cut}} (\text{keV})$	20 ± 5	19^{+6}_{-2}	24^{+4}_{-3}	27^{+6}_{-5}
C_{bat}	$0.23^{+0.08}_{-0.05}$	$0.18^{+0.07}_{-0.03}$	1.18 ± 0.14	1.28 ± 0.11
C_{xis1}			1.09 ± 0.03	1.09 ± 0.03
C_{hxd}			0.92 ± 0.13	0.92 ± 0.15
$E_{\text{cyc}} (\text{keV})$		32 ± 4		30 ± 5
D_c		0.6 ± 0.2		0.45 ± 0.17
$\chi^2_{\text{red}} (\text{d.o.f.})$	1.41 (106)	1.18 (104)	1.24 (133)	1.12 (131)
	fdco			
N_{H}	$7.3^{+1.5}_{-1.3}$	$6.0^{+1.1}_{-1.2}$	8.0 ± 0.6	7.8 ± 0.6
Γ	0.9 ± 0.3	0.6 ± 0.3	1.28 ± 0.12	1.24 ± 0.11
$N_{\text{po}} (10^{-3})$	12^{+10}_{-5}	5.2 ± 0.8	5.8 ± 0.6	5.3 ± 1.1
$E_{\text{fol}} (\text{keV})$	18^{+5}_{-3}	19^{+4}_{-3}	22^{+3}_{-2}	24^{+4}_{-3}
$E_{\text{cut}} (\text{keV})$	< 7.4	< 20	< 8	< 22
C_{bat}	$0.22^{+0.08}_{-0.05}$	0.18 ± 0.05	1.13 ± 0.11	$1.24^{+0.22}_{-0.17}$
C_{xis1}			1.10 ± 0.03	1.10 ± 0.03
C_{hxd}			0.90 ± 0.13	0.91 ± 0.15
$E_{\text{cyc}} (\text{keV})$		32.4 ± 3.5		31 ± 5
D_c		0.6 ± 0.2		0.50 ± 0.17
$\chi^2_{\text{red}} (\text{d.o.f.})$	1.48 (105)	1.21 (103)	1.33 (132)	1.17 (130)
	npex			
N_{H}	$7.3^{+1.1}_{-1.3}$	$5.8^{+1.2}_{-1.0}$	7.7 ± 0.6	7.5 ± 0.5
Γ	$0.81^{+0.15}_{-0.3}$	0.45 ± 0.3	$1.05^{+0.1}_{-0.6}$	1.01 ± 0.16
$E_{\text{cut}} (\text{keV})$	$15.3^{+0.7}_{-2.7}$	16^{+6}_{-4}	16^{+4}_{-2}	17^{+6}_{-1}
$N_n^a (10^{-8})$	$6.4^{+1.7}_{-4.7}$	< 70	$1.3^{+0.2}_{-0.9}$	$1.0^{+0.5}_{-0.9}$
$N_n^b (10^{-3})$	$6.1^{+2.8}_{-2.4}$	3.1 ± 0.1	2.4 ± 0.5	2.2 ± 0.4
C_{bat}	$0.28^{+0.06}_{-0.08}$	0.20 ± 0.06	1.35 ± 0.14	1.41 ± 0.18
C_{xis1}		1.10 ± 0.03	1.10 ± 0.03	
C_{hxd}		1.06 ± 0.15	1.04 ± 0.16	
$E_{\text{cyc}} (\text{keV})$		33 ± 4		31^{+8}_{-12}
D_c		0.5 ± 0.2		$0.30^{+0.19}_{-0.14}$
$\chi^2_{\text{red}} (\text{d.o.f.})$	1.32 (105)	1.16 (103)	1.16 (132)	1.10 (130)

Notes. ^(a) Normalization of the power-law with positive index
^(b) Normalization of the power-law with negative index

were found marginally worse with respect to the models with the `cyclabs` component.

The best-fitting value of C_{bat} is ~ 0.2 . We verified that this value is consistent with the intensity of the BAT light curve during the XRT observation, a factor ~ 4 higher than the average source intensity along the 54 months of monitoring.

We show in Fig. 1 data of *Spectrum 1* and residuals for the models of first/second columns of Table 1.

3.2. Spectrum 2

We used the pointed Suzaku observation to perform a complementary analysis, checking how a different soft X-ray spectrum could affect the shape of the hard X-ray spectrum. The analysis was performed in analogy with the steps described for *Spectrum 1*. The third and fourth column of Table 1 show the results of the spectral fitting for the three models, with and without the addition of the cyclotron line. The results are well in agreement with those obtained for *Spectrum 1*. Again, the best-fitting model of the continuum emission is found for the `npex` model. For this model, the normalisation constant C_{bat} is ~ 1.4 . A value that is ~ 6 times higher with respect to *Spectrum 1*; the observed flux

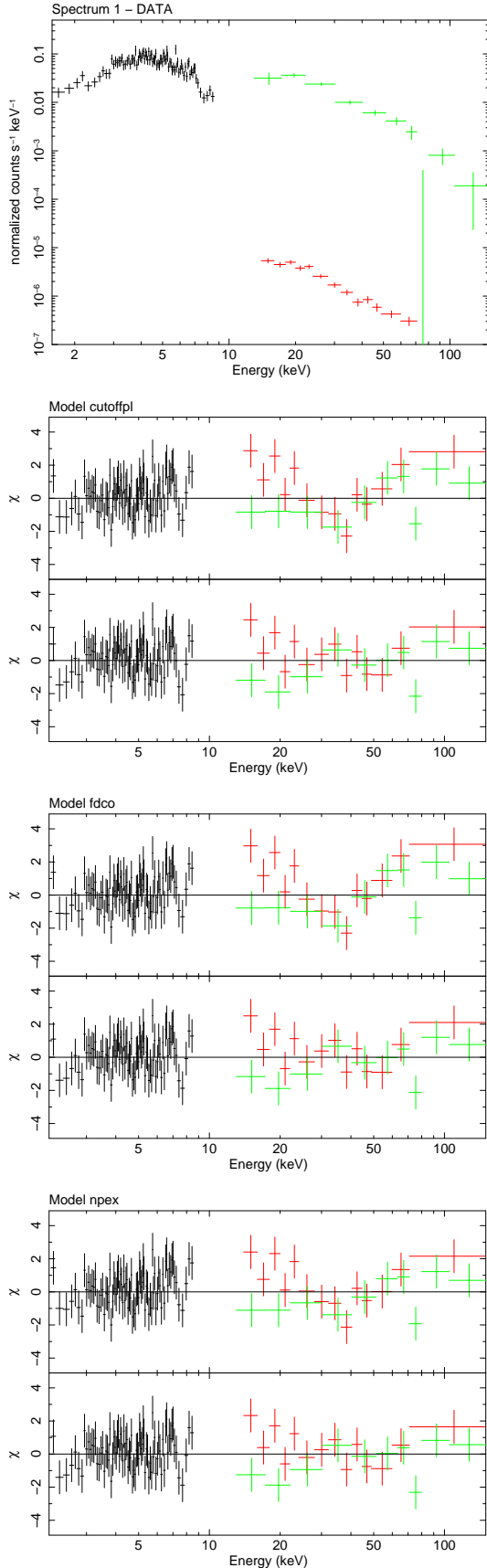


Figure 1. Upper panel: datasets that compose the *Spectrum 1* analysis. Black data: XRT spectrum; red data: BAT spectrum; green data: ISGRI spectrum. Lower panels: residuals in units of σ for the continuum models of Table 1; upper mid-panels: only continuum, lower mid-panels: continuum with the addition of a cyclotron absorption feature at ~ 31 keV.

during the Suzaku observation is, in fact, ~ 4 times less with respect to the XRT observation. Despite the drop in the soft X-ray flux no statistically significant variation in the spectral shape of the emission is observed. Best-fitting values for the two spectra are in agreement, although the power-law steepness is only marginally compatible, indicating during the Suzaku observation a possible softer X-ray spectrum.

The best fit to the continuum emission (*npex* model) gave a reduced $\chi^2 = 1.16$ (132 d.o.f.), while the model with the *cyclabs* component gave a reduced $\chi^2 = 1.10$ (130 d.o.f.). The line shape is found to depend only marginally on the soft X-ray band. The cyclotron line parameters are, however, less constrained with respect to *Spectrum 1*, although best-fitting values remain well consistent. We show in Fig.2 data of *Spectrum 2* and residuals for the models of third and fourth column of Table 1.

3.3. Calibration uncertainties of the BAT instrument

Because the detection of the cyclotron features is mostly pivoted by the BAT high-energy data, we checked for possible biases in the analysis due to incorrect background subtraction or systematics in the BAT response matrix⁴ by comparing the extracted spectrum of IGR J16493–4348 with the spectra of nearby X-ray sources having similar spectral shape.

We selected from the 54-months BAT catalogue the three HMXBs closest to IGR J16493–4348: IGR J16393-4643, IGR J16418-4532 and AX J1700.2-4220. We extracted the BAT long-term spectra and used pointed Swift-XRT and XMM-Newton (Epic-PN spectrum for AX J1700.2-4220) to obtain their broadband X-ray spectra. The spectra of IGR J1639.1-4641 and AX J1700.2-4220 could be well fitted using a cut-off power-law model, while the spectrum of IGR J16418-4532 required a *npex* model to be satisfactorily fitted. In each case the BAT data did not show any structure in the residuals in the 30–40 keV range. Because of the similarity in the shape of the continuum emission, the common background estimate, and the comparable statistics in the BAT data among all the sources of this sample and IGR J16493–4348, we conclude that the residuals shown in the spectrum of IGR J16493–4348 cannot be due to calibration uncertainties of the BAT instrument nor to an incorrect estimate, or subtraction, of the X-ray background.

3.4. A method for testing the significance of the detection

To estimate the statistical significance of the residuals present in the BAT data of IGR J16493–4348, we adopted the following procedure (see also Suchy et al. 2011 for a similar approach):

- we assumed the best-fitting *npex* model for *Spectrum 1* in Table 1 without the cyclotron line as the *null-hypothesis model*;
- we simulated accordingly a faked BAT spectrum having the same S/N ratio of the real BAT spectrum;
- we fitted again the datasets of *Spectrum 1* (real data and simulated BAT spectrum) using the *npex* model with and without the addition of an absorption cyclotron line (width constrained at 10 keV, with line energy and optical depth as free parameters);
- we calculated the difference in $\Delta\chi^2$ for the two best-fitting models: *npex* and *npex+cyclabs*;

⁴ http://swift.gsfc.nasa.gov/docs/swift/analysis/bat_digest.html

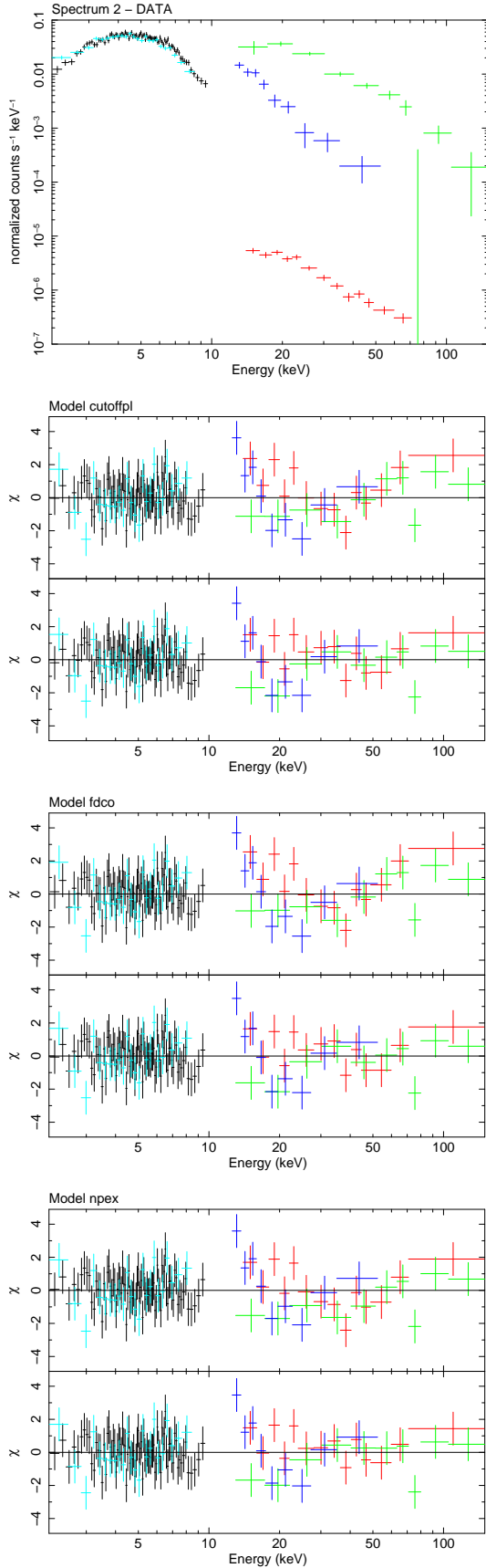
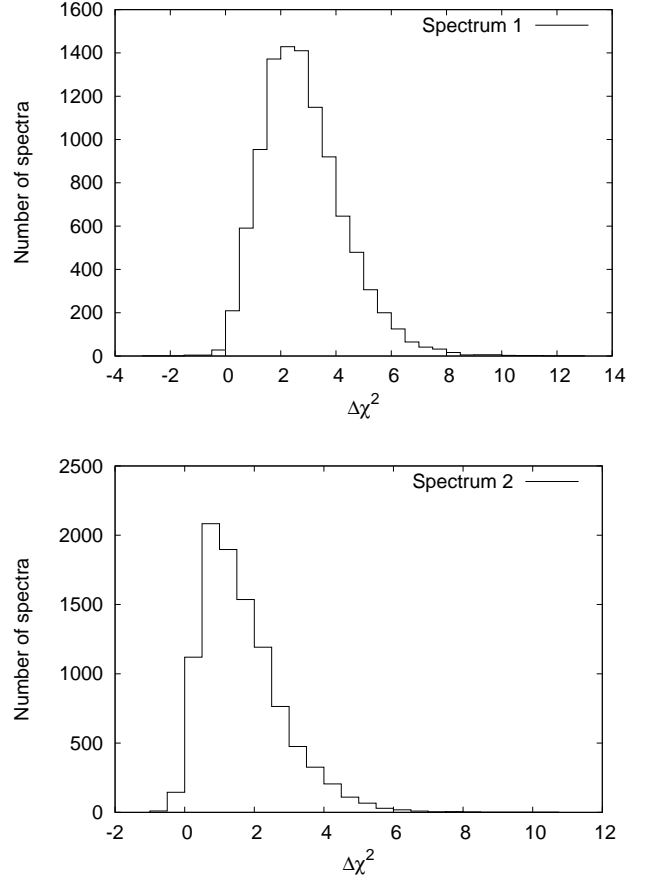


Figure 2. Upper panel: datasets that compose the *Spectrum 2* analysis. Black data: XIS023 spectrum; red data: BAT spectrum; green data: ISGRI spectrum; blue data: Suzaku/HXD-PIN spectrum; light blue: XIS0 spectrum. Lower panels: residuals in units of σ for the continuum models of Table 1; upper mid-panels: only continuum, lower mid-panels: continuum with the addition of a cyclotron absorption feature at ~ 31 keV.

Figure 3. Histograms of the difference in $\Delta\chi^2$ obtained fitting the datasets of *Spectrum 1* and *Spectrum 2*, when the real BAT spectrum is substituted with a BAT simulated spectrum. The χ^2 difference is calculated for the two best-fitting models: *npex* and *npex+cyc*.



- we repeated this procedure for other 10,000 faked BAT spectra;
- we plotted with histograms the $\Delta\chi^2$ difference versus the number of spectra;
- we repeated the same procedure for the *Spectrum 2* datasets;

In Fig. 3, we show the results of our method. In 10,000 spectra we did not obtain any difference in the $\Delta\chi^2$ as the ones reported in Table 1, both for the *Spectrum 1* (observed $\Delta\chi^2=19$) and for the *Spectrum 2* (observed $\Delta\chi^2=10$) datasets. The shape of the distribution is different in the two cases: the XRT data constrain less the broadband shape and the addition of a broad feature in absorption in most cases improves the fit. On the contrary the Suzaku data are less sensible to fitting improvements even for the addition of a broad, continuum-like, feature. This is expected since the statistical weight of the Suzaku XIS ($\sim 20,000$ counts in the XIS spectra versus the $\sim 2,000$ counts of the XRT spectrum) data more strongly pivot the overall determination of the continuum shape and the χ^2 result. At the same time, tighter constraints of the continuum shape make random fluctuations as artifacts less probable. We note, therefore, that the detection level as estimated from the difference in the χ^2 of the two models (with and without the addition of the cyclotron absorption feature) in *Spectrum 2* real data, although in absolute value

less than what found for *Spectrum 1*, is consistent and in agreement with the detection level obtained from *Spectrum 1* data. Moreover, we have estimated this detection level for the model (n_{pex}) that provided the lowest improvements for the addition of this features; the other spectral models would have given a much higher detection confidence. Because from the generation of 10,000 simulated spectra no random fit improvement of the same order, or greater, than the one we obtained from real data was obtained for both datasets, we estimate a detection level corresponding to at least ~ 3.9 gaussian sigmas for the presence of a cyclotron line in our fits.

4. Discussion

There are 15 sources that clearly have shown CRSFs signatures in their spectra. This number represents about 10% of the total population of HMXBs detected in our Galaxy (Reig 2011) and, despite the considerable amount of observing time dedicated by modern and past X-ray observatories, to this class of sources, new detections of CRSFs have not considerably risen in the last decade.

We have presented new results based on the analysis of the data collected by BAT during the first 54 months of the *Swift* mission on a persistent sgHMXB IGR J16493–4348. We have shown that the long-term BAT collected hard X-ray spectra provides an access for detecting the presence of CRSFs in this kind of sources. This new approach relies on a series of assumptions and caveats that will be hereinafter discussed.

The broadband spectrum, modelled with a positive-negative cut-off power-law model provides the statistically most favoured description of the data in the examined datasets. The residuals in the BAT energy range show the presence of an absorption feature between ~ 28 and ~ 38 keV. The feature is not sensibly dependent on the adopted soft X-ray contribution, although we have just exploited the only two available to date pointed observations with XRT and Suzaku. The broad negative residuals are compatible with a resonant cyclotron absorption feature with an estimated significance of the detection at least at $\sim 4\sigma$ level.

Similar features are often seen in the high energy spectra of sgHMXB. They are interpreted as cyclotron lines produced near the magnetic poles of the accretion-powered neutron star. These are due to resonant scattering processes of the X-rays by electrons whose kinetic energies are quantised in discrete Landau energy levels perpendicular to the B-field. Their detection is fundamental for the understanding of the accretion mechanisms unto the neutron star as it allows a direct measurement of the magnetic field of the neutron star (or at least a lower limit, depending on the height where the resonant line absorption is effectively produced, see Nishimura 2011).

We consider here that the cyclotron absorption takes place at the poles of the neutron star, taking into account the relativistic gravitational redshift: $E_{\text{cyc}}^{\text{obs}} = E_{\text{cyc}}(1+z)^{-1}$, with

$$(1+z)^{-1} = \left(1 - \frac{2GM_X}{R_X c^2}\right)^{0.5} \quad (2)$$

Assuming typical values for the NS mass and radius (1.4 M_{\odot} and 10 km, respectively) and the observed value of the cyclotron line energy of 33 ± 4 keV (n_{pex} model for *Spectrum 1*), this implies a magnetic field of $B_{\text{NS}} (3.7 \pm 0.4) \times 10^{12}$ Gauss at the surface of the NS.

The energy resolution of the spectra is not sufficient to independently constrain line energy, line width and depth. Because

the line energy and depth could be relatively better constrained with respect to the line width, we choose to freeze this value to 10 keV. This value represents a first-order guess assumed in consideration of the emerging relations among the parameters that characterize the cyclotron line shapes. An empirical correlation between line energy and line width (Coburn et al. 2002) is, in fact, observed, where cyclotron lines detected between 30 keV and 40 keV show preferably line widths in the 5–10 keV range (e.g. in MX 0656-072, 4U 0352+309, XTE J1946+274, [see Coburn et al. (2002); McBride et al. (2006)]). We tried in all the fittings also to freeze the line width at 5 keV and 8 keV to check how sensible was the determination of this parameter. We generally found that the 10 keV guess always provided the lowest χ^2 , even if the improvements in most cases were marginal ($2 < \Delta\chi^2 < 5$). Another important empirical correlation concerns the cut-off energies of the continuum emission and the cyclotron line energy, where a correlation is observed with cut-off energies typically at half the value of the cyclotron energy. Also in this case, our results appear in agreement with the general trend that is observed, with a cut-off energy at ~ 15 keV and the cyclotron energy at \sim two times this value (Heindl et al. 2004).

Possible biases in this analysis are envisaged by the use of long-term time averaged spectra for features that may show some variability. Some luminosity-dependent shifts of the cyclotron line position were in fact clearly observed in some sources (Mihara et al. 2004; Staubert et al. 2007; Nakajima et al. 2010). However the large uncertainties in the present analysis estimates do not allow to set this possibility into investigation. IGR J16493–4348 has never shown unusual periods of strong changes in its luminosity, nor any outbursting behavior as in the case of X0331+53, where luminosity changed by a factor ~ 200 (Nakajima et al. 2010), so that we argue that possible shifts, if present, should be within our quoted error-bars. Moreover, it is to be noted that the cyclotron feature at 45 keV of A0535+262 did not show any variations despite a change in luminosity of two orders of magnitude (Terada et al. 2006). Another source of bias concerns the possibility of continuum spectral changes, that, when averaged, could result in spectral artifacts. The analysis of the soft X-ray spectrum from the XRT and Suzaku pointed observations are not sufficient to test any variability pattern in the broadband spectral properties; use of simplified, phenomenological, models are also possible source of bias and a more physically based model should be employed to also infer the physical properties of the accretion column environment (Becker & Wolff 2007; Schönherr et al. 2007) and to better constrain the shape of cyclotron resonance features.

4.1. Conclusions

We have presented spectral analysis in the high-energy X-ray band of IGR J16493–4348 using long-term survey data from BAT and ISGRI, complemented with pointed soft X-ray observations from XRT and Suzaku. The BAT spectrum is to date the highest S/N spectrum of this source in the high-energy X-ray band. When the spectrum is complemented with soft X-ray data, a broad absorption feature is detected, irrespective of the broadband model used to fit the data. We modeled the feature assuming that it is a CRSF. This interpretation is statistically acceptable and the physical interpretation of the parameters is in agreement with what expected from the whole sample of HMXBs that show similar features. We estimated the significance level of the detection $> 3.9\sigma$ confidence level and next generation of future observatories dedicated to the high X-ray band (e.g. NuSTAR and Astro-H) will likely provide a more stringent confirm of its

presence and a substantial improvement in the determination of its shape.

Acknowledgements

The authors acknowledge financial contribution from the agreement ASI-INAF I/009/10/0

References

- Barthelmy, S. D., Barbier, L. M., Cummings, J. R., et al. 2005, *Space Sci. Rev.*, 120, 143
- Becker, P. A. & Wolff, M. T. 2007, *ApJ*, 654, 435
- Bird, A. J., Barlow, E. J., Bassani, L., et al. 2004, *ApJ*, 607, L33
- Boldt, E. 1987, *Phys. Rep.*, 146, 215
- Burrows, D. N., Hill, J. E., Nousek, J. A., et al. 2005, *Space Sci. Rev.*, 120, 165
- Coburn, W., Heindl, W. A., Rothschild, R. E., et al. 2002, *ApJ*, 580, 394
- Corbet, R. H. D. 1984, *A&A*, 141, 91
- Corbet, R. H. D., Pearlman, A. B., & Pottschmidt, K. 2010, *The Astronomer’s Telegram*, 2766, 1
- Cusumano, G., La Parola, V., Romano, P., et al. 2010a, *MNRAS*, 406, L16
- Cusumano, G., La Parola, V., Segreto, A., et al. 2010b, *A&A*, 510, A48+
- Fukazawa, Y., Mizuno, T., Watanabe, S., et al. 2009, *PASJ*, 61, 17
- Gehrels, N., Chincarini, G., Giommi, P., et al. 2004, *ApJ*, 611, 1005
- Grebenev, S. A., Bird, A. J., Molkov, S. V., et al. 2005, *The Astronomer’s Telegram*, 457, 1
- Heindl, W. A., Rothschild, R. E., Coburn, W., et al. 2004, in *American Institute of Physics Conference Series*, Vol. 714, *X-ray Timing 2003: Rossi and Beyond*, ed. P. Kaaret, F. K. Lamb, & J. H. Swank, 323–330
- Hill, A. B., Dean, A. J., Landi, R., et al. 2008, *MNRAS*, 385, 423
- Hill, J., Burrows, D., Nousek, J., et al. 2004, *APS Meeting Abstracts*, 10005
- Koyama, K., Tsunemi, H., Dotani, T., et al. 2007, *PASJ*, 59, 23
- Kuiper, L., Jonker, P., Hermsen, W., & O’Brien, K. 2005, *The Astronomer’s Telegram*, 654, 1
- Makishima, K., Mihara, T., Ishida, M., et al. 1990, *ApJ*, 365, L59
- Makishima, K., Mihara, T., Nagase, F., & Tanaka, Y. 1999, *ApJ*, 525, 978
- McBride, V. A., Wilms, J., Coe, M. J., et al. 2006, *A&A*, 451, 267
- Mihara, T., Makishima, K., & Nagase, F. 2004, *ApJ*, 610, 390
- Mitsuda, K., Bautz, M., Inoue, H., et al. 2007, *PASJ*, 59, 1
- Morris, D. C., Smith, R. K., Markwardt, C. B., et al. 2009, *ApJ*, 699, 892
- Nakajima, M., Mihara, T., & Makishima, K. 2010, *ApJ*, 710, 1755
- Nespoli, E., Fabregat, J., & Mennickent, R. E. 2010, *A&A*, 516, A106+
- Nishimura, O. 2011, *ApJ*, 730, 106
- Reig, P. 2011, *Ap&SS*, 332, 1
- Schönherr, G., Wilms, J., Kretschmar, P., et al. 2007, *A&A*, 472, 353
- Segreto, A., Cusumano, G., Ferrigno, C., et al. 2010, *A&A*, 510, A47+
- Staubert, R., Shakura, N. I., Postnov, K., et al. 2007, *A&A*, 465, L25
- Suchy, S., Pottschmidt, K., Rothschild, R. E., et al. 2011, *ArXiv e-prints*
- Takahashi, T., Abe, K., Endo, M., et al. 2007, *PASJ*, 59, 35
- Terada, Y., Mihara, T., Nakajima, M., et al. 2006, *ApJ*, 648, L139